ARMY RESEARCH LABORATORY

Coupled CFD/GN&C Modeling for a Smart Material Canard Actuator

by Paul Weinacht

ARL-TR-4265 **September 2007**

NOTICES

Disclaimers

The findings in this report are not to be construed as an official Department of the Army position unless so designated by other authorized documents.

Citation of manufacturer's or trade names does not constitute an official endorsement or approval of the use thereof.

Destroy this report when it is no longer needed. Do not return it to the originator.

Army Research Laboratory
Aberdeen Proving Ground, MD 21005-5066

ARL-TR-4265 **September 2007**

Coupled CFD/GN&C Modeling for a Smart Material Canard Actuator

Paul Weinacht
Weapons and Materials Research Directorate, ARL

REPORT DOCUMENTATION PAGE	Form Approved OMB No. 0704-0188

1. REPORT DATE *(DD-MM-YYYY)*	2. REPORT TYPE	3. DATES COVERED (From - To)
September 2007	Final	2003–2005

4. TITLE AND SUBTITLE
Coupled CFD/GN&C Modeling for a Smart Material Canard Actuator

5a. CONTRACT NUMBER

5b. GRANT NUMBER

5c. PROGRAM ELEMENT NUMBER

6. AUTHOR(S)
Paul Weinacht

5d. PROJECT NUMBER
1L1612618AH

5e. TASK NUMBER

5f. WORK UNIT NUMBER

7. PERFORMING ORGANIZATION NAME(S) AND ADDRESS(ES)
U.S. Army Research Laboratory
ATTN: AMSRD-ARL-WM-BC
Aberdeen Proving Ground, MD 21005-5066

8. PERFORMING ORGANIZATION REPORT NUMBER
ARL-TR-4265

9. SPONSORING/MONITORING AGENCY NAME(S) AND ADDRESS(ES)

10. SPONSOR/MONITOR'S ACRONYM(S)

11. SPONSOR/MONITOR'S REPORT NUMBER(S)

12. DISTRIBUTION/AVAILABILITY STATEMENT
Approved for public release; distribution is unlimited.

13. SUPPLEMENTARY NOTES

14. ABSTRACT
The performance of a smart material canard actuator has been investigated using coupled computational fluid dynamics, guidance, navigation and control, and structural models. The predictions show that the open-loop response of the smart material actuator does not produce the commanded deflection due to the interaction of the externally applied aerodynamic hinge moment with the flexible actuator structure. A closed-loop feedback control law with integral control is applied in order for the canard to attain the commanded deflection. However, the predictions show that the gain for the integral controller must be correctly selected to obtain the proper response of the canard. The selected gain is dependent on both the structural characteristics of the actuator and the applied aerodynamics.

15. SUBJECT TERMS
aerodynamics, aeroballistics, smart materials, CFD, GN&C

16. SECURITY CLASSIFICATION OF:			17. LIMITATION OF ABSTRACT	18. NUMBER OF PAGES	19a. NAME OF RESPONSIBLE PERSON
a. REPORT	b. ABSTRACT	c. THIS PAGE			Paul Weinacht
UNCLASSIFIED	UNCLASSIFIED	UNCLASSIFIED	UL	30	19b. TELEPHONE NUMBER (*Include area code*) 410-306-0782

Contents

List of Figures

List of Tables

Acknowledgments

Portions of this work were supported by a grant of computer time from the Department of Defense High Performance Computing Major Shared Resource Center at the U.S. Army Research Laboratory. The element-based GN&C model utilized here was developed by Professor Mark Costello of the Georgia Institute of Technology (previously from Oregon State University) as part of the computer program BOOM, a computer-aided engineering tool for exterior ballistics of smart projectiles. Portions of this code were integrated by the author into the CFD code utilized in the current study. The smart cargo projectile configuration used in the current study was designed and conceived by Wilfredo Toledo of the U.S. Army Armament Research, Development, and Engineering Center, and has been used in several studies as a representative conceptual design for a gun-launched canard-controlled munition.

INTENTIONALLY LEFT BLANK.

1. Introduction

The U.S. Army Research Laboratory is currently investigating smart munitions technologies as a means of improving the lethality and accuracy of future generations of munitions. One of the focuses of the current effort is the development of integrated multidisciplinary design technologies such as structural dynamics, computational fluid dynamics (CFD), and guidance, navigation, and control (GN&C). These multidisciplinary design technologies allow complex munition systems to be studied and visualized within high-performance computational environments to determine the nonlinear interaction of critical engineering parameters using high-fidelity physics. This allows detailed design trades to be performed on system subcomponents, resulting in reduced development costs and higher performance munitions.

As part of this effort, the performance of a smart materials canard actuator has been investigated using a multi-disciplinary design approach. Figure 1 shows a schematic of the design examined as part of the current study, although this represents only one of many possible approaches.[1] The canard itself is a hollow aeroshell structure that pivots about a rotational hinge that is attached to the main body and canard aeroshell. The hinge is strategically located to minimize the hinge moments. In the design shown in figure 1, the hinge has been located near the canard mid-chord position close to the expected location of the canard center of pressure for supersonic flight. To provide actuation of the fin, two beams consisting of piezoelectric material have been placed inside the aeroshell. These beams are attached to the munition body and to the outer tip of the canard aeroshell. The internal geometry of the aeroshell provides enough clearance so that when the beams are deflected in an opposing manner, the canard rotates about the hinge, providing a deflection of the canard. By incorporating the canard actuator within the canard aeroshell, volume intrusion of the GN&C package into the munition payload is minimized.

The early phases of the actuator design process focused on static (steady-state) performance of the canard actuator. Important design considerations included the development of actuator concepts capable of producing the required canard deflection angles while producing enough available torque to overcome the externally applied aerodynamic torque. The computational capability discussed here was utilized in this phase of the effort to determine the magnitude and variability of the applied aerodynamic hinge moments across the flight envelope as well as to minimize their effect by proper location of the hinge itself.

In the current phase of the investigation, the time-dependent dynamic response of the smart material canard actuator has been investigated by applying a coupled CFD/GN&C/structural model to the candidate configuration. The CFD approach allows the instantaneous aerodynamic

[1] Rabinovitch, O.; Vinson, J. R. Smart Fins: Analytical Modeling and Basic Design Concepts. *Mechanics of Advanced Materials and Structures* **2003**, *10* (3), 249–269.

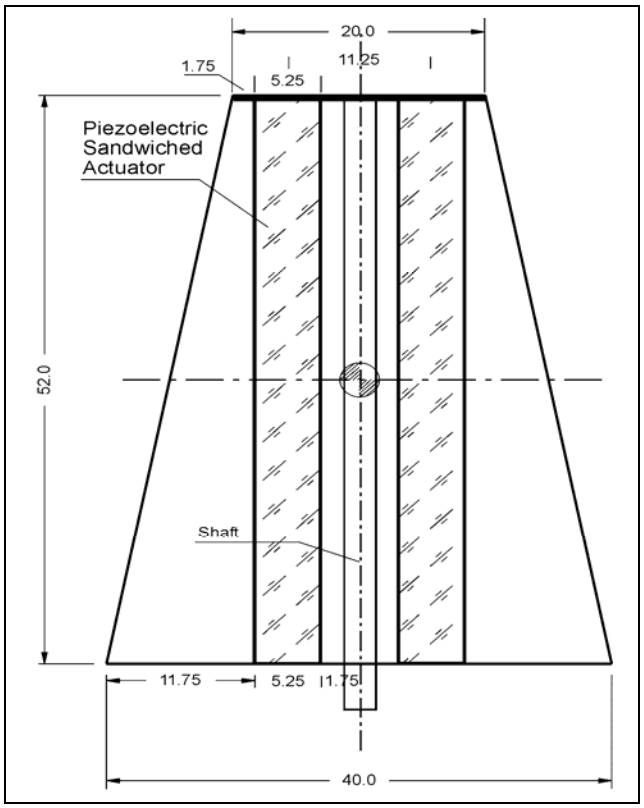

Figure 1. Candidate smart material canard actuator design.

torque acting on the canard surface to be accurately determined due to the combined effects of angle of attack, canard deflection, and canard deflection rate. Using the instantaneous aerodynamic torque derived from CFD, the canard motion is subsequently determined from solutions of the rigid body equations of motion of the canard structure, the control laws, and the structural modeling of the piezoelectric actuator in a fully coupled manner. A description of the computational modeling approach is presented in the following section.

A generic smart cargo munition has been chosen as a candidate vehicle for the smart material canard actuator. Figure 2 shows a schematic of the smart cargo munition. The munition has four deflecting canards on the nose of the projectile, with four fixed tail fins. To accurately determine the aerodynamic loads on the canard including the interference effect of the body on the canard, the aerodynamic flow field for the complete munition body has been simulated. In the current report, results are first presented examining the open-loop performance of the canard actuator system in the presence of aerodynamic torque. The open-loop results demonstrate the need for feedback control of the flexible canard actuator system due to the externally applied aerodynamic torque. Closed-loop control with feedback and integral control are then presented. The effect of variations in the gain for the integral controller is examined and the results demonstrate that acceptable performance of the canard actuator can be obtained by the appropriate selection of the integral controller gain.

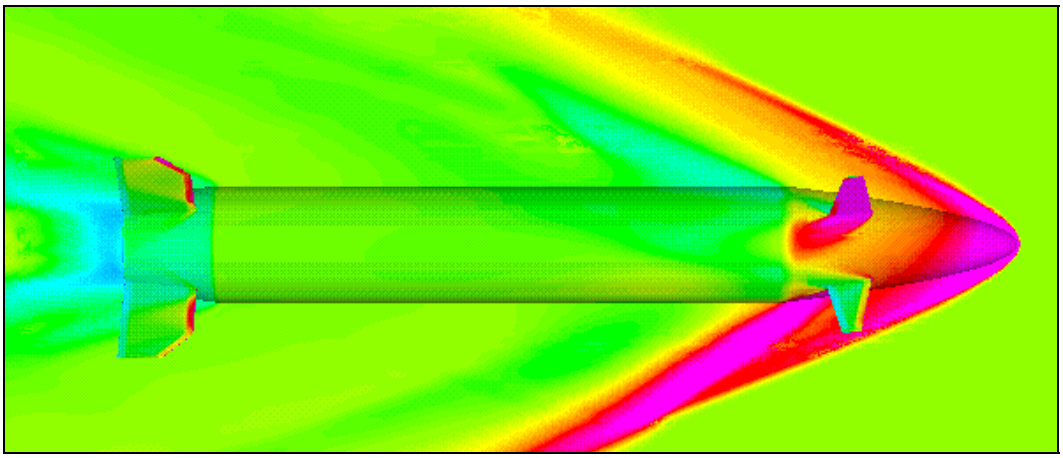

Figure 2. Generic smart cargo munition.

2. Computational Approach

The flow field about the canard-controlled smart munition has been predicted using an overset grid approach[2, 3] that allows relative motion between bodies in close proximity. The method utilizes a near-body grid system of interconnecting grids that conform to various pieces of the bodies surrounded by an outer off-body Cartesian-based grid system. The interconnecting near-body grids overlap and intergrid connectivity is established using a Chimera overset gridding approach. This significantly reduces the demands on grid generation, as each body component can be gridded independently. The outer off-body Cartesian grid system encompasses the near-body grid system and extends to the outer boundary of the computational domain. The off-body grid system typically consists of several levels of grid refinement, with the most refined grids in proximity to the near-body grids and increasingly less refined grids further away from the body.

Figure 3 shows the near-body and a portion of the off-body grid systems used for the computation. The surface grids for the near-body grid system is shown in figure 4. For the main body, four grids were used. These included a main-body grid, a nose-cap grid, a grid that wrapped around the base corner, and a simple Cartesian grid along the base axis to remove the base axis singularity. For each canard, four additional grids were utilized. The four grids included a main canard grid, tip and root-cap grids, and a box grid encompassing the main canard grid and the tip and root-cap grids. A closeup of the canard grids is shown in figure 5. A similar grid structure was used for the fin grids, shown in figure 6, with the exception that the

[2]Renze, K. J.; Buning, P. G.; Ragagopalan, R. G. *A Comparative Study of Turbulence Models for Overset Grids*; AIAA Paper No. 92-0437, January 1992.

[3]Meakin, R. L. *A New Method for Establishing Inter-grid Communication Among Systems of Overset Grids*; AIAA Paper No. 91-1586, June 1991.

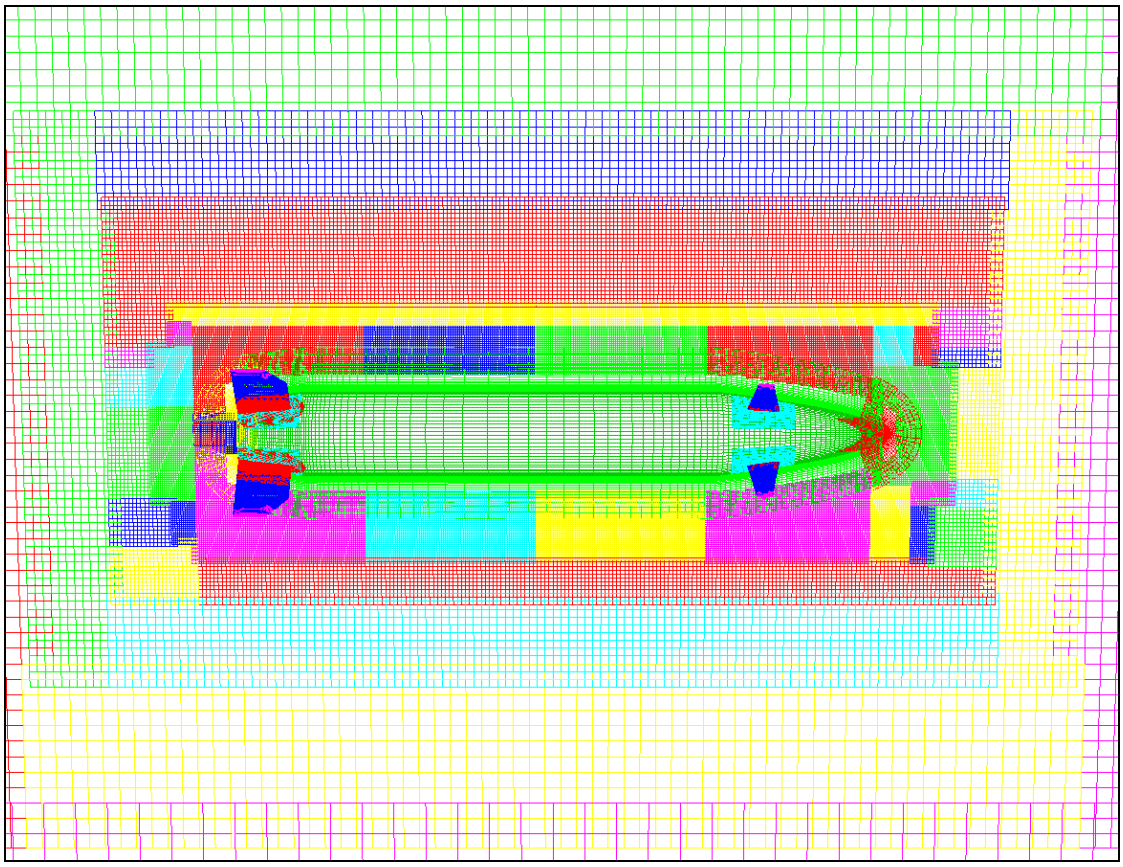

Figure 3. Near-body and off-body grid system.

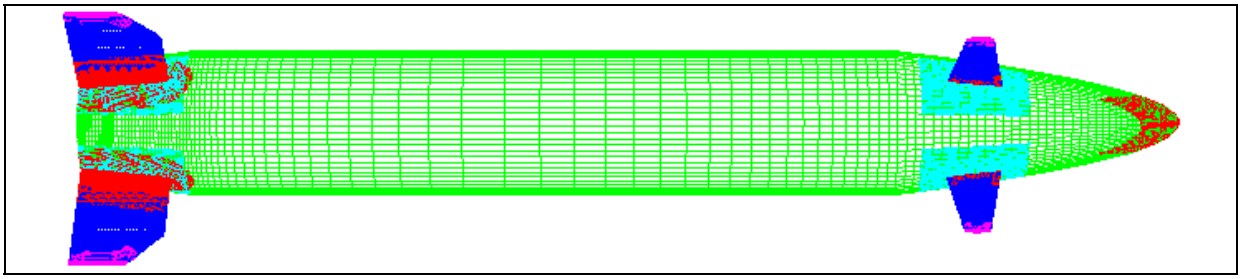

Figure 4. Near-body surface grid.

fin-collar grid was used for the permanently mounted fins in place of the root-cap grid used on the canards. Approximately 10.9-million grid points were used in the complete CFD grid system with 1.2-million points used in near-body grid systems encompassing each of the canards.

Solution of the compressible Reynolds-averaged Navier-Stokes equations is accomplished using a three-factor, diagonal-implicit, first-order accurate time-stepping scheme that employs second-order accurate central differencing in space. The Baldwin-Barth one-equation turbulence model has been utilized. Characteristics-based inflow/outflow boundary conditions have been applied on the boundaries of the domain. On the body surface, no-slip, adiabatic boundary conditions are imposed.

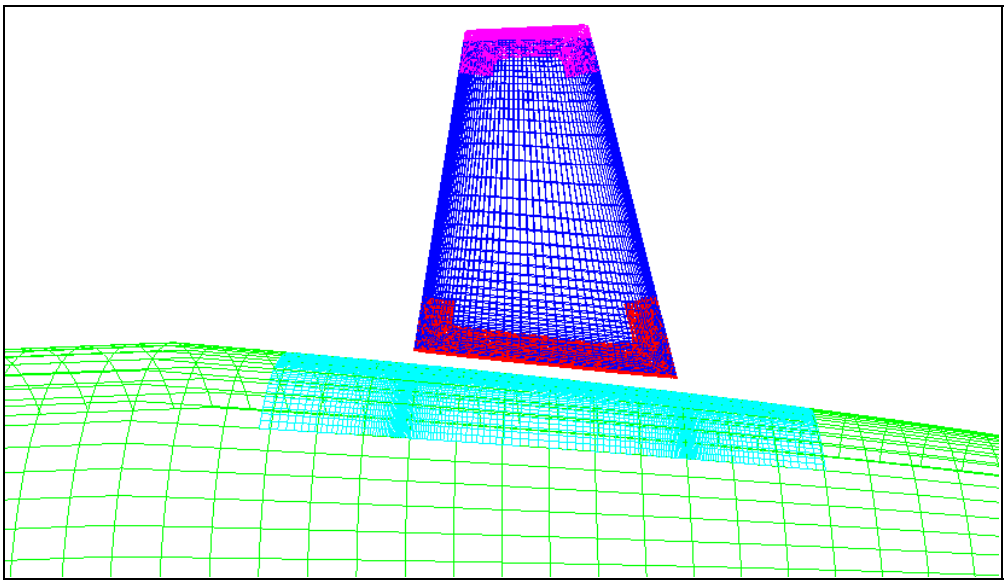

Figure 5. Near-body surface grid near canard.

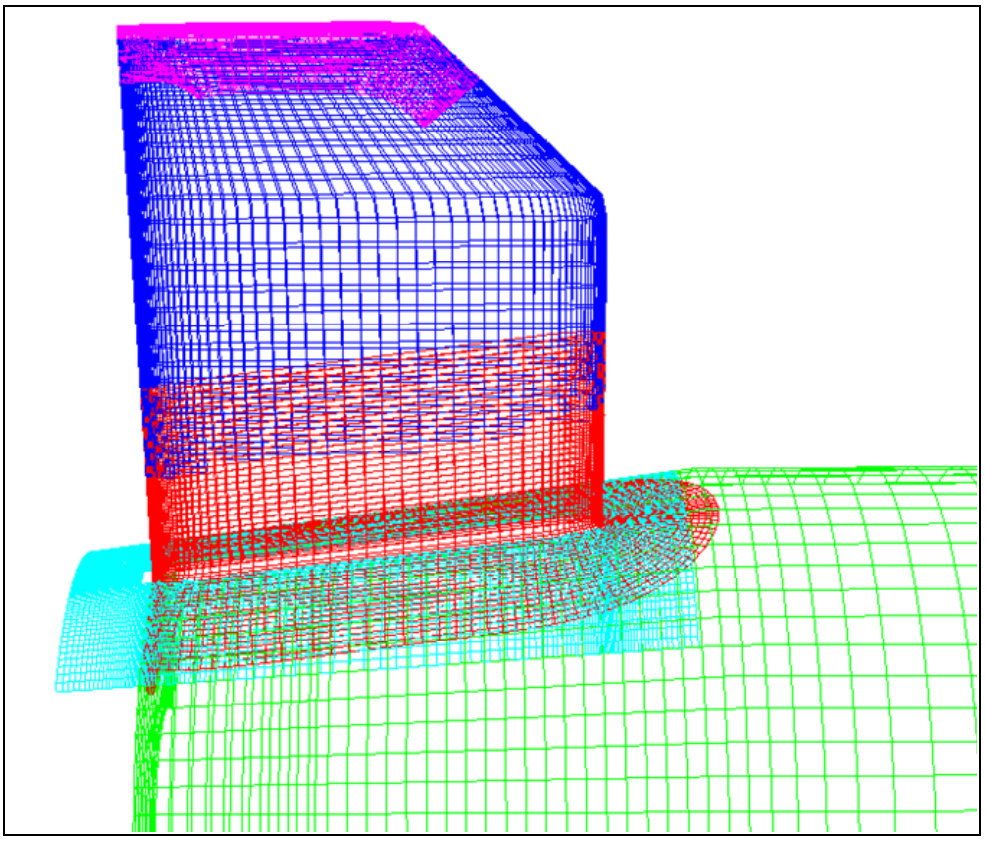

Figure 6. Near-body surface grids near tailfins.

The original code also included a six degree of freedom (6-DOF) rigid-body dynamics (RBD) capability for coupled CFD and RBD calculations. Using an interface provided within the code, the original 6-DOF RBD capability was replaced with a generalized 6-DOF RBD and GN&C capability. The GN&C capability employs an element-based approach for constructing complex control schemes and includes common fundamental control elements such as summers, comparators, gains, and integrators, as well as more advanced components such as proportional navigation elements. For the current application, the GN&C capability allows control schemes for the canard actuator to be easily constructed so that the canard deflection can be controlled.

The results from analysis based on classical plate and lamination theories and constitutive modeling of the piezoelectric material have been used to characterize the structural response of the smart material actuator.[1] For the current framework, the results are used to determine the appropriate torsional spring constant of the smart material canard actuator structure. Consistent with the applied theory, the available applied torque from the canard actuator varies linearly with the applied voltage.

The aerodynamics, RBD, control, and structural response are fully coupled in the computational method and the contributions of each are evaluated at each time step of the computation. Although the implementation allows inner iteration at each time step, this feature was not applied in the current computations. Approximately 15,000 time steps were used in each of the current simulations. The bulk of the computational time was consumed in the evaluation of the aerodynamics and addition of the control and RBD added little to the overall computational cost.

3. Results

The computational capability was applied to examine the time-dependent response of the smart material canard actuator. For the computations presented here, the initial state of the projectile was fixed at 0° angle of attack and a flight velocity of Mach 2. The initial deflection angle of the canards was also fixed at 0°. The initial conditions represent the initial state of the projectile prior to a commanded maneuver. The deflection of the canard is initiated with a commanded deflection of 10°. The focus of the investigation was the response of the canard itself as part of an overall maneuver. However, the time scale of the canard response is necessarily smaller than the response time of the munition. Only the response of the canard itself is examined here, although the technique is capable of predicting the resulting response of the complete munition.

When the smart material canard actuator is deflected on the laboratory benchtop, it is possible to obtain a calibration of the necessary voltage to obtain a desired deflection. With this calibration, it is possible to command a particular deflection and the canard will produce the desired deflection after a finite response time that is determined by the inertial properties of the canard and actuator system. However, in flight, there is an additional external torque that is applied to the canard actuator system from the aerodynamic torque acting on the external surface of the aeroshell. This aerodynamic torque is variable and completely dependent on the flight condition of the projectile, i.e., flight velocity, angle of attack, and canard deflection angle.

The control diagram for the open-loop response is shown in figure 7. The two primary inputs and outputs of the control loop are the commanded deflection of the canard δ_{IN} and the instantaneous deflection of the canard $\delta(t)$, respectively. The aerodynamic torque T_{AERO} represents an external disturbance to the system and dependent on the external state of the projectile, specifically, the flight Mach number, angle of attack, and roll angle. The dynamic response of the canard is represented by the plant model and is a function of the moment of inertia of the canard about the hinge axis, I, the damping produced by the friction in the hinge, V, and the elastic response of the smart material actuator represented by the torsional spring constant K. Parameters used for the current computations are shown in table 1.

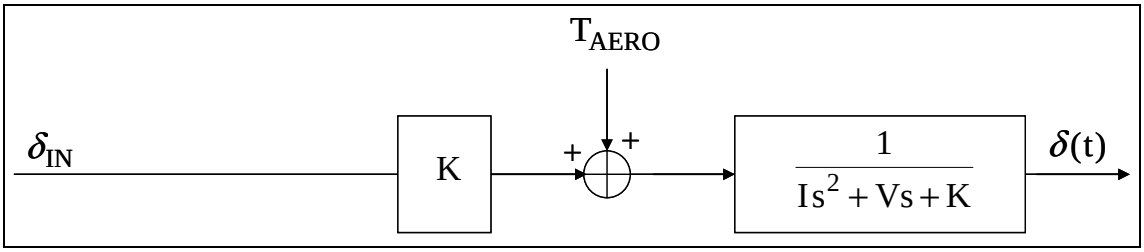

Figure 7. Control diagram for open-loop response.

Table 1. Canard actuator physical properties.

I, Canard moment of inertia about hinge (kg-mm^2)	0.5866
K, Torsional spring constant (N-m/rad)	0.52888
V, Frictional damping coefficient (N-m-s/rad)	1899.0

Figure 8 shows the predicted open-loop (no feedback) response of the canard using the multidisciplinary computational approach for a commanded deflection of 10° from an initial canard deflection angle of 0°. Because of the inertial properties of the canard, the deflection takes about 0.5 ms to reach its steady-state deflection of about 5°. This is only half of the commanded response because of the aerodynamic torque that opposes the applied torque of the canard actuator. For the open-loop system, the steady-state response of the canard is dependent on the local flow conditions and a different response will be obtained if the angle of attack or Mach number is changed. Clearly, this will not provide adequate controllability for the canard and the munition.

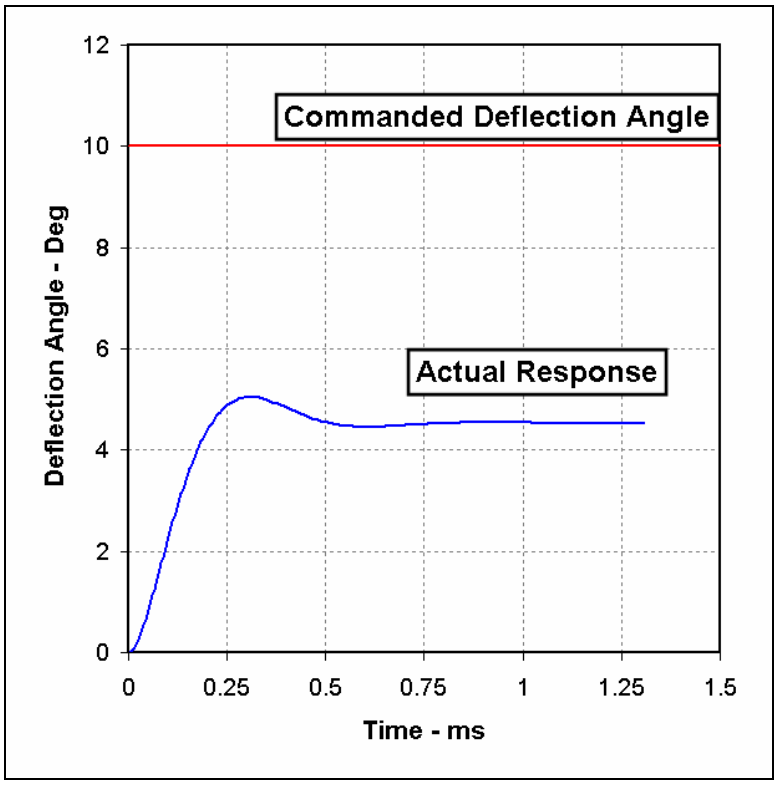

Figure 8. Open-loop response of canard.

The desired response of the canard can be obtained through the use of feedback control. Feedback control allows additional voltage to be applied to the canard actuator so that the commanded deflection is obtained. Figure 9 shows the feedback control loop used for controlling the canard in the current study. The feedback control loop contains several blocks that characterize the response of the canard. Again, the two primary inputs and outputs of the control loop are the commanded deflection of the canard δ_{IN} and the instantaneous deflection of the canard $\delta(t)$, respectively. The feedback of the time-dependent canard deflection $\delta(t)$ occurs on the lower leg of the control loop. Although not specifically modeled in the current simulation, smart materials themselves could be utilized as a sensor for feedback of the instantaneous canard deflection as part of the current actuator design. A comparator extracts the difference between the commanded deflection and the instantaneous canard deflection and sends the output through an integral control element. The integral control element contains a gain I_C that controls the amplitude of the output of the integral control element. This gain must be properly specified to obtain acceptable control. The output from the integral control element is summed with the external aerodynamic torque that is subsequently input to the final control element which characterizes the dynamic behavior of the canard. This dynamic behavior includes the inertial, mechanical damping, and elastic properties of the smart material actuator. It should be noted that the external aerodynamic torque is the instantaneous torque and includes

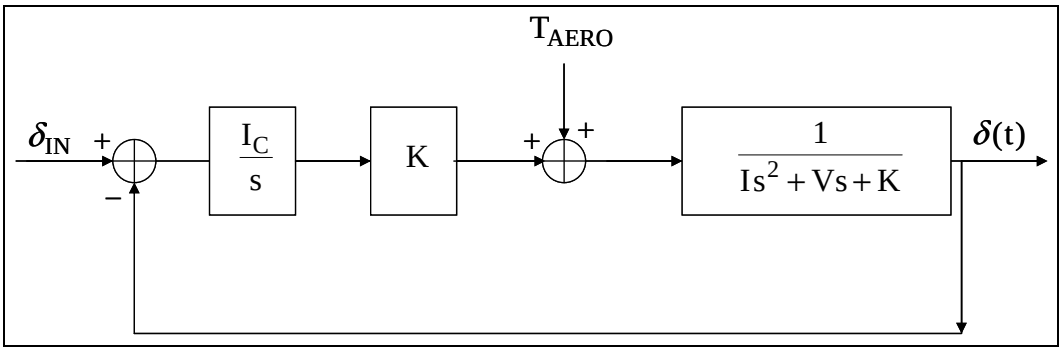

Figure 9. Control diagram for closed-loop response.

contributions from both the static and dynamic aerodynamic moments. The aerodynamic torque also serves as an input to the control loop; however, the torque represents an external disturbance to the system that acts independently to the operation of the system.

A series of computational results of the response of the smart material canard actuator with closed-loop feedback was obtained for different levels of integral controller gain I_C. Figure 10 shows the predicted response of the canard with the feedback control and an optimal value of the integral controller gain. The commanded canard deflection is obtained to within half a degree after about 0.5 ms with the steady-state response obtained at about 1.0 ms. There is little under- or over-shoot in the predicted response. Even with the integral control, there is still some time lag in the response because of the inertial properties of the fins. Using the feedback control law with an appropriately selected gain, the smart material actuator should provide adequate control for the munition.

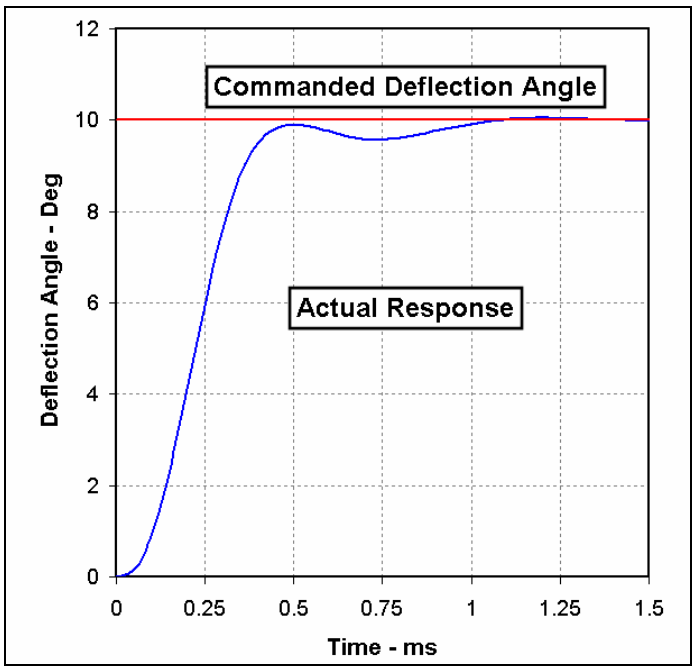

Figure 10. Closed-loop response, I_C = 10,000/s.

Figure 11 shows the response of the canard with the gain for the integral controller set too low. Here, the canard eventually obtains the commanded canard deflection, but the response is slower than desired, and the canard may not be able to provide the munition with adequate control. However, if the gain for the integral controller is too high, the system becomes overdriven. As shown in figure 12, the response is oscillatory, and, if the gain is high enough, the response is divergent. The results shown here clearly demonstrate that the gain for the integral controller plays an important role in the response of the canard.

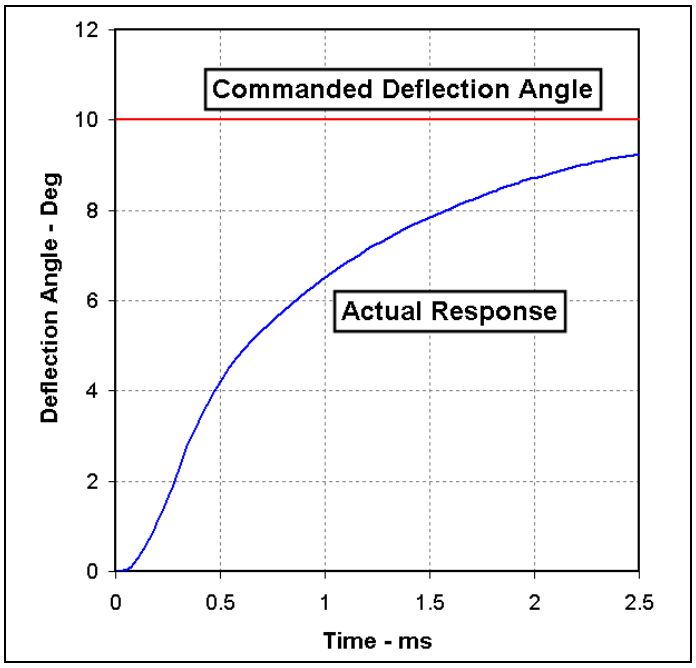

Figure 11. Closed-loop response with low gain, I_C = 2500/s.

An important design consideration for the smart material canard actuator is the applied torque that must be produced by the actuator so that the commanded deflection can be obtained. The applied torque produced by the smart material canard actuator can be determined using the predicted results. The applied torque for the open-loop response is simply the product of the torsional spring constant and the commanded deflection as shown in equation 1.

$$T_{applied} = K\delta_{IN}. \quad (1)$$

For the steady-state response of the smart material canard actuator in the absence of an applied aerodynamic torque, the applied torque counteracts the torsional stiffness of the actuator beams to produce the commanded deflection. However, in the presence of aerodynamic loads, the applied torque has to overcome both the aerodynamic torque and the torsional stiffness of the actuator beams. Thus, the actual steady-state deflection is typically less than the commanded

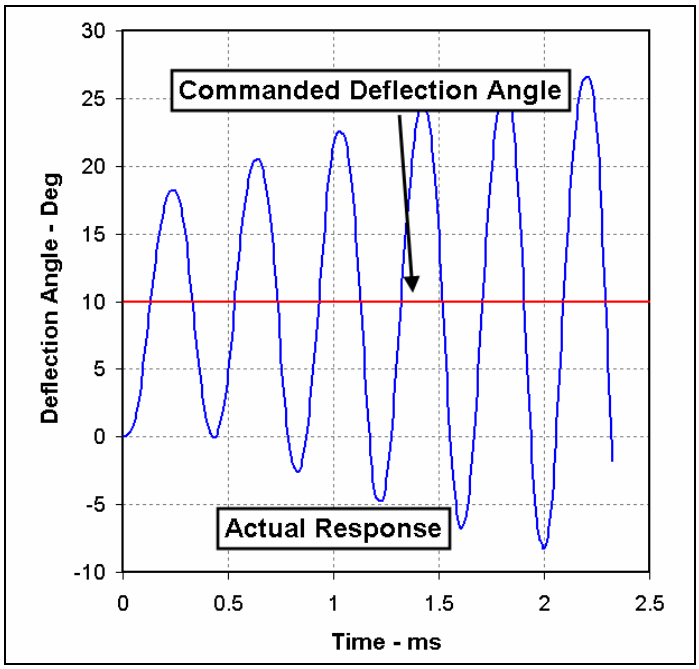

Figure 12. Closed-loop response with high gain, I_C = 65,000/s.

deflection. For the closed-loop response, the applied torque is adjusted through the use of the integral controller in order produce the commanded deflection. The time-dependent response of the applied torque can be computed using equation 2.

$$T_{applied} = KI_C \int_0^t (\delta_{IN} - \delta(t))dt \, . \qquad (2)$$

Figure 13 shows the applied torque as a function of time for the case where the gain is 10,000 (1/s). Also shown is the applied torque for the open-loop case. The integral controller increases the applied torque as a function of time until the commanded deflection is attained. There is very little overshoot in the applied torque which implies that the use of the integral controller does not significantly increase the maximum applied torque requirements for the smart material actuator compared with torque required to attain the steady-state commanded deflection. The applied torque for the closed-loop case is increased (in this case nearly doubled) compared with the open-loop applied torque due to the additional torque requirement from the aerodynamic torque. In the absence of any aerodynamic torque, the open-loop applied torque is sufficient to produce the commanded deflection.

A significant benefit of the coupled approach is that the instantaneous aerodynamic torque is utilized to determine the response of the smart material canard actuator. The predicted aerodynamic torque includes all the relevant instantaneous effects, including canard deflection angle, deflection rate, and angle of attack of the munition subject to the full three-dimensional

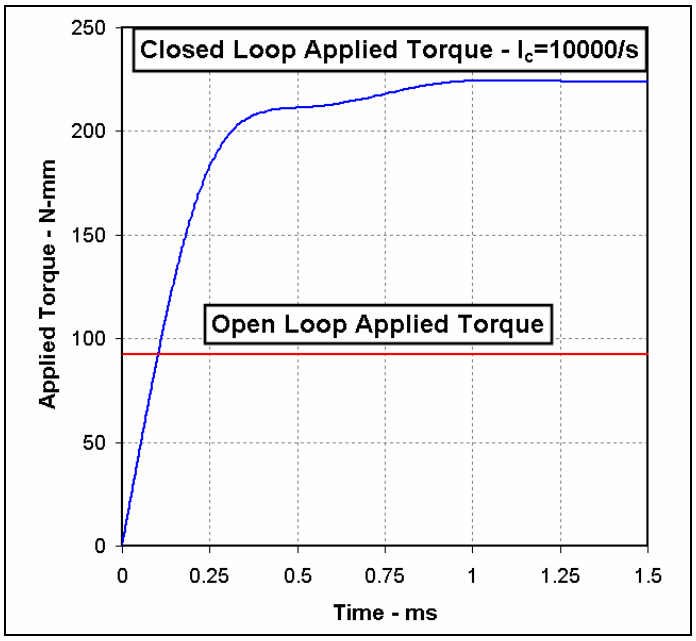

Figure 13. Applied torque for optimal gain.

interference effects of the body. There is no assumed form for the aerodynamic torque as the computational approach produces a single integrated value for the aerodynamic torque which represents all of the combined effects. The downside of the coupled approach is that parametric studies can be computationally intensive because the aerodynamic computation (the largest computational expense) needs to be performed for each case. Some of the computational expense of these parametric studies can be reduced by modeling the relevant aerodynamic effects using the computational results as a guide. This requires that the aerodynamic torque be modeled using an assumed functional form and the parameters defining this functional form be evaluated using the CFD predictions. Such analysis was performed as part of this study.

For the case of 0° angle of attack, the following linear aerodynamic model for the aerodynamic hinge moment can be proposed:

$$T_{AERO} = K_{m_\delta}\delta + K_{m_{\dot\delta}}\left(\frac{\dot\delta\,\ell}{V_\infty}\right) = \left[C_{m_\delta}\delta + C_{m_{\dot\delta}}\left(\frac{\dot\delta\,\ell}{V_\infty}\right)\right]\frac{1}{2}\rho V_\infty^2 S_{ref}\,\ell\,. \qquad (3)$$

This model accounts for the aerodynamic moments due to both the canard deflection angle δ and the canard deflection angular rate $\dot\delta$. The rate is nondimensionalized by the flight velocity V and the characteristic length ℓ, which is chosen here as the projectile body diameter. Additional aerodynamic moment contributions may be present if the projectile is at angle of attack; however, these are not included for the current analysis.

The equation of motion for the open-loop response can be written as shown in equation 4.

$$I\ddot{\delta} + V\dot{\delta} + K\delta = K\delta_{IN} + T_{AERO}\,. \tag{4}$$

Using this model for the aerodynamic moment, the equation of motion for the open-loop response can be written as shown in equation 5.

$$\ddot{\delta} + \frac{V - K_{m_{\dot{\delta}}}\left(\frac{\ell}{V_\infty}\right)}{I}\dot{\delta} + \frac{K - K_{m_\delta}}{I}\delta = \frac{K}{I}\delta_{IN}\,. \tag{5}$$

Equation 5 is a second-order ordinary differential equation with constant coefficients. The solution is shown in equation 6.

$$\delta(t) = \delta_{IN}\frac{K}{I(a^2 + b^2)}\left(1 - \exp(bt)\cos(at) + \frac{b}{a}\exp(bt)\sin(at)\right), \tag{6}$$

where

$$a = \sqrt{\frac{K - K_{m_\delta}}{I} - \left(\frac{V - K_{m_{\dot{\delta}}}\left(\frac{\ell}{V_\infty}\right)}{2I}\right)^2}\,, \tag{7}$$

and

$$b = -\frac{V - K_{m_{\dot{\delta}}}\left(\frac{\ell}{V_\infty}\right)}{2I}\,. \tag{8}$$

The analytical solution of the governing equation 6 can be used to determine both of the aerodynamic moments by fitting the computed open-loop response (shown previously in figure 8) using a nonlinear least-squares approach to determine the parameters a and b. Using the fitted response, the aerodynamic moment coefficients C_{m_δ} and $C_{m_{\dot{\delta}}}$ can be extracted using equations 7 and 8. Figure 14 shows both the computed open-loop response and the fitted result using equation 6. The fitted result is a good representation of the computed response. From the fit of the open-loop response, it was determined that $C_{m_\delta} = -0.00241$ and $C_{m_{\dot{\delta}}} = -0.00234$. The value of C_{m_δ} determined from the fitting was very close to the predicted C_{m_δ} from static computations of the canard deflection at 5° canard deflection angle. Additionally, these static predictions showed a generally linear trend with canard deflection angle although some slight nonlinearity was observed for canard deflection angles approaching 10°. Nonetheless, the static torque using C_{m_δ} from the fitted open-loop response was within 15% of the predicted static torque over the range of canard deflection angles between –15 and +15°. The closed-loop response can also be fit in a similar manner to determine the aerodynamic coefficients but the fitting procedure is more complicated because of the complex form of the analytical solution for the closed-loop solution which is the basis of the fitting procedure.

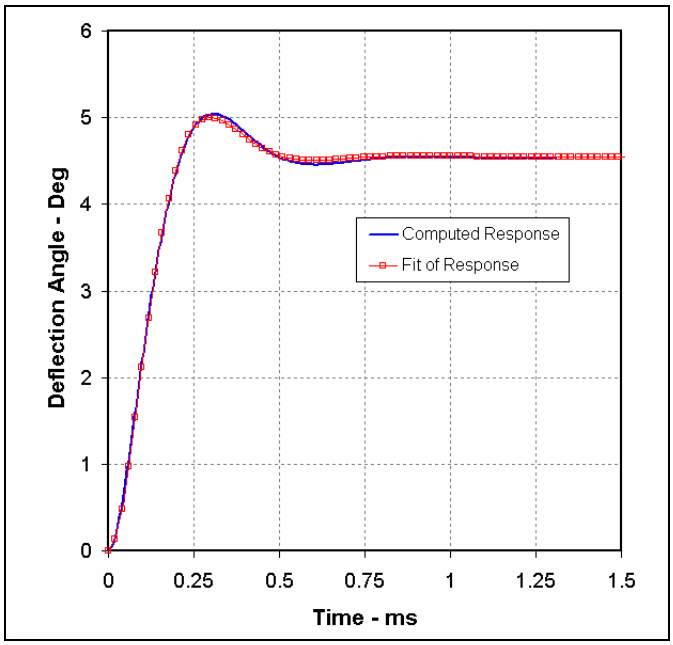

Figure 14. Comparison of computed motion and fit of computed motion.

Using these estimates for the aerodynamic coefficients, analytical solutions for the closed-loop response were obtained and compared with the response obtained from the coupled computational procedure. Figure 15 shows a comparison of the actuator response from the coupled computation and the results of the closed-form solution obtained using the aerodynamic coefficients determined from the open-loop response. The results show good agreement. However, when the solutions for higher gain (I_C = 35,000/s) are compared, as shown in figure 16, some variation between the two sets of results is noted. In particular, the frequency of the response for the modeled aerodynamics is higher, and the damping rate is lower. The results demonstrate that the approximate model is not universally valid, particularly for the off-design conditions. Thus, the full multidisciplinary design capability is needed to accurately assess the response of the smart material canard actuator across a more complete range of conditions.

The analytical solution can also be used to determine the relative importance of the aerodynamic damping. Figure 17 shows a comparison of the open-loop response predicted using the coupled simulation and the analytical solution without the aerodynamic damping included. Without aerodynamic damping, the response is oscillatory. The oscillatory motion is damped due the small amount of frictional/structural damping. Without aerodynamic damping, additional frictional/structural damping would likely be needed to improve the open loop performance. The aerodynamic damping plays a similar role in the closed-loop performance. Figure 18 shows a comparison of the closed-loop response predicted using the coupled simulation and the analytical solution of the closed-loop performance with no aerodynamic damping. In this case, the

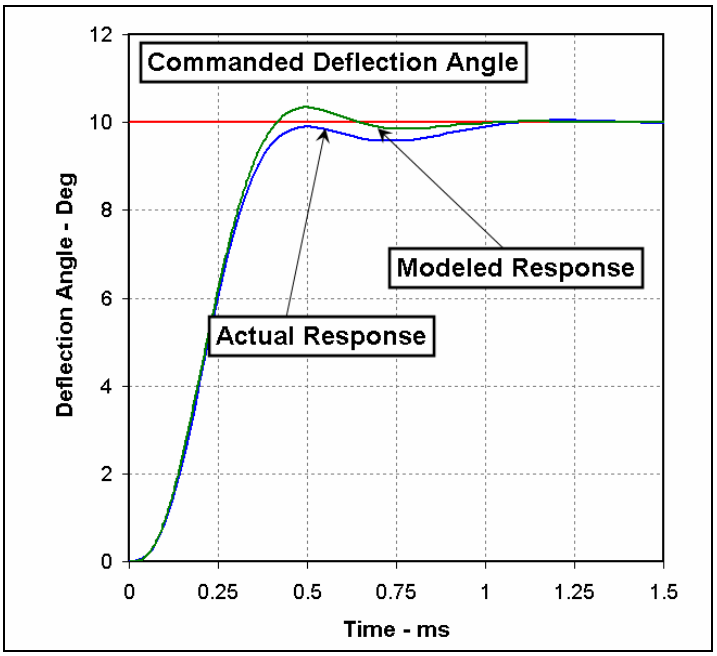

Figure 15. Comparison of closed-loop actuator response from coupled simulation and analytical solution using modeled aerodynamic torque, I_C = 65,000/s.

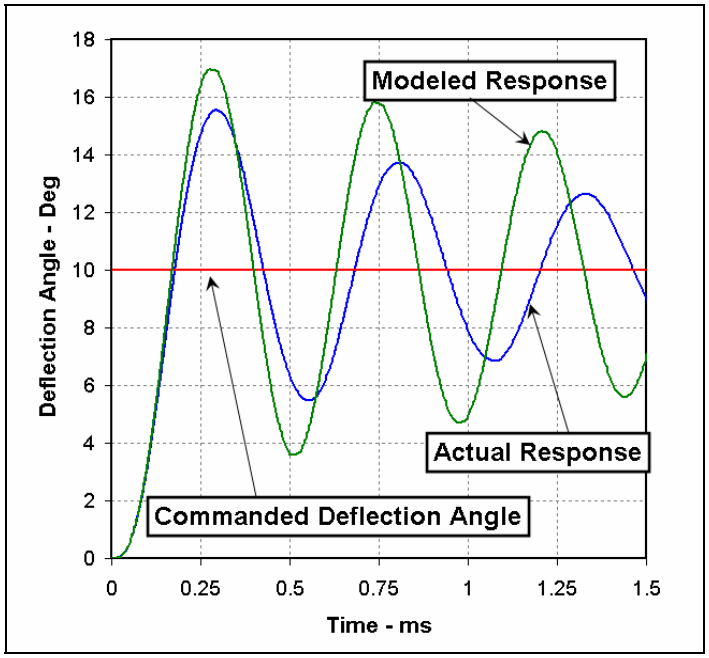

Figure 16. Comparison of closed-loop actuator response from coupled simulation and analytical solution using modeled aerodynamic torque, I_C = 35,000/s.

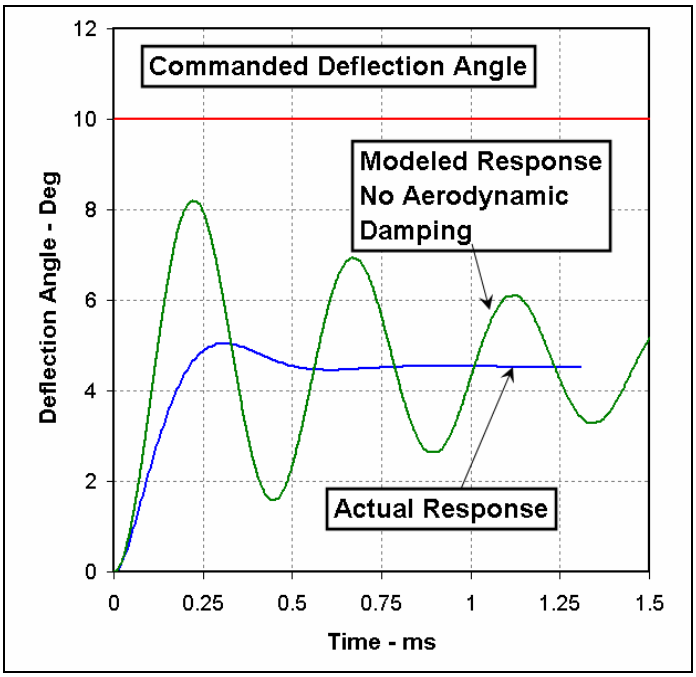

Figure 17. Comparison of open-loop actuator response from coupled simulation and analytical solution with no aerodynamic damping.

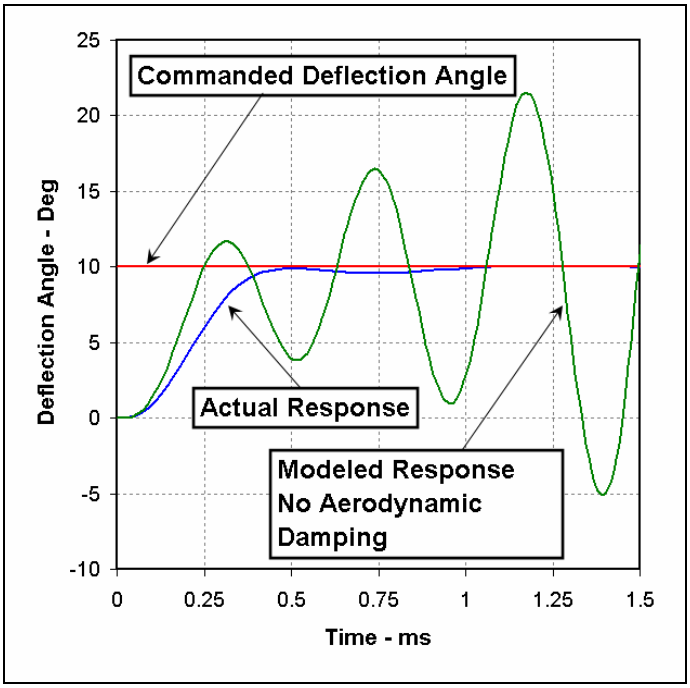

Figure 18. Comparison of closed-loop actuator response from coupled simulation and analytical solution with no aerodynamic damping, I_C = 10,000/s.

response with no aerodynamic damping is unstable. Thus, for the range of parameters examined here, the aerodynamic damping must be considered when the actuator performance is modeled, and, in particular, when the integral controller gain is selected. The results also imply that the integral controller gain is sensitive to the rate-dependent aerodynamics because the rate-dependent aerodynamics provide additional damping for the system.

4. Conclusion

Using a multidisciplinary approach, the time-dependent response of a smart material actuator concept has been evaluated. The results show that a closed-loop feedback control law is required to produce the desired deflection because of the interaction of the externally applied aerodynamic loads with the flexible structure that is inherently part of the smart material actuator design. The multidisciplinary approach provides a means of properly designing and tuning the control law to provide optimal control of the canard actuator system. This demonstrates the utility of the approach as a sophisticated but cost-effective means of evaluating control strategies for future munition systems.

List of Symbols, Abbreviations, and Acronyms

C_{m_δ}	Variation of nondimensional aerodynamic torque with canard deflection angle
$C_{m_{\dot{\delta}}}$	Variation of nondimensional aerodynamic torque with canard deflection angular rate
I	Moment of inertia of canard about hinge axis
I_C	Gain for integral controller
K	Torsional spring constant
K_{m_δ}	Variation of dimensional aerodynamic torque with canard deflection angle
$K_{m_{\dot{\delta}}}$	Variation of dimensional aerodynamic torque with canard deflection angle
ℓ	Reference length based on munition diameter
S_{ref}	Reference area for aerodynamic coefficients based on munition cross-sectional area
t	Time
T_{AERO}	Aerodynamic torque
$T_{applied}$	Applied torque
V	Structural damping coefficient
V_∞	Freestream air velocity

Greek Symbols

δ_{IN}	Commanded canard deflection angle
$\delta(t)$	Instantaneous canard deflection angle
$\dot{\delta}$	Angular velocity of canard deflection
$\ddot{\delta}$	Angular acceleration of canard deflection
ρ	Freestream air density

NO. OF
COPIES ORGANIZATION

1 (PDF ONLY) DEFENSE TECHNICAL INFORMATION CTR
DTIC OCA
8725 JOHN J KINGMAN RD
STE 0944
FORT BELVOIR VA 22060-6218

1 US ARMY RSRCH DEV & ENGRG CMD
SYSTEMS OF SYSTEMS INTEGRATION
AMSRD SS T
6000 6TH ST STE 100
FORT BELVOIR VA 22060-5608

1 DIRECTOR
US ARMY RESEARCH LAB
IMNE ALC IMS
2800 POWDER MILL RD
ADELPHI MD 20783-1197

3 DIRECTOR
US ARMY RESEARCH LAB
AMSRD ARL CI OK TL
2800 POWDER MILL RD
ADELPHI MD 20783-1197

ABERDEEN PROVING GROUND

1 DIR USARL
AMSRD ARL CI OK TP (BLDG 4600)

NO. OF COPIES ORGANIZATION

1 US MILITARY ACADEMY
MATH SCI CTR EXCELLENCE
MADN MATH
THAYER HALL
WEST POINT NY 10996-1786

3 U OF NEVADA, LAS VEGAS
M TRABIA
W YIM
B O'TOOLE
DEPT OF MECH ENG
LAS VEGAS NV 89154-4027

1 ALLIANT TECHSYSTEMS INC
R DOHRN
MN11 1428
600 SECOND ST NE
HOPKINS MN 55343

1 AFRL MNAV
G ABATE
STE 219
101 W EGLIN BLVD
EGLIN AIR FORCE BASE FL 32542

1 DEFENSE INTELLIGENCE AGENCY
MISSILE & SPACE INT CTR
MSA1 A NICHOLSON
BLDG 4545
FOWLER RD
REDSTONE ARSENAL AL 35898-5500

1 AEROPREDICTION INC
F MOORE
STE 201
9449 GROVER DR
KING GEORGE VA 22485

1 ATK LAKE CITY
SMALL CALIBER AMMUN
LAKE CITY ARMY AMMUN PLANT
D MANSFIELD
PO BOX 1000
INDEPENDENCE MO 64051-1000

1 ALLIANT TECHSYSTEMS INC
D KAMDAR
MN11 2830
600 SECOND ST NE
HOPKINS MN 55343

NO. OF COPIES ORGANIZATION

1 ALLIANT TECHSYSTEMS INC
R BECKER
MN11 2626
5050 LINCOLN DR
EDINA MN 55340-1097

2 DIRECTOR
NASA AMES RESEARCH CTR
MS 2581 B MEAKIN
MS T27B2 M AFTOSMIS
MOFFETT FIELD CA 94035

1 DIRECTOR
NASA LANGLEY RES CTR
TECH LIB
LANGLEY STATION
HAMPTON VA 23665

1 COMMANDER
NSWC
CODE 420
A WARDLAW
INDIAN HEAD MD 20640-5053

1 COMMANDER
NSWC
CODE B40
W YANTA
DAHLGREN VA 22448-5100

1 US ARMY TACOM ARDEC
AMSRD AAR AEW M(D)
M D MINISI
BLDG 65 N
PICATINNY ARSENAL NJ 07806-5000

2 USAF WRIGHT AERONAUTICAL LAB
AFWAL FIMG
J SHANG
N E SCAGGS
WPAFB OH 45433-6553

1 MIT
TECH LIB
77 MASSACHUSETTS AVE
CAMBRIDGE MA 02139

1 DIRECTOR
SANDIA NATIONAL LAB
DIV 1554
W OBERKAMPF
ALBUQUERQUE NM 87185

NO. OF COPIES	ORGANIZATION
1	US ARMY TACOM ARDEC AMSRD AAR AEM I R MAZESKI BLDG 61 N PICATINNY ARSENAL NJ 07806-5000
1	US ARMY TACOM ARDEC AMSRD AAR AEM A A FARINA BLDG 95 PICATINNY ARSENAL NJ 07806-5000
3	ARROWTECH ASSOC W HATHAWAY R WHYTE M STEINHOFF 1233 SHELBURNE RD STE D8 SOUTH BURLINGTON VT 05403
1	COMMANDER USAAMCOM AMSAM RD SS G LANDINGHAM REDSTONE ARSENAL AL 35898-5252
1	UNIV OF TEXAS DEPT OF AERO ENG D DOLLING AUSTIN TX 78712-1055
4	COMMANDER US ARMY TACOM ARDEC AMSTA AR FSF T C NG J GRAU W KOENIG W TOLEDO BLDG 382 PICATINNY ARSENAL NJ 07806-5000
1	GEORGIA INST OF TECH DEPT OF AEROSPACE ENG M COSTELLO ATLANTA GA 0332
1	COMMANDER US ARMY TACOM ARDEC LOS/BLOS AMSTA AR CCH B P VALENTI BLDG 354 PICATINNY ARSENAL NJ 07806-5000

NO. OF COPIES	ORGANIZATION
1	DIRECTOR US ARMY RSCH LAB AMSRD ARL RO EN T DOLIGALSKI RSCH TRIANGLE PARK NC 27703
3	CDR USAMCOM AMSAM RD MG J BAUMANN J LOCKER AMSRD AMR SG SD B NOURSE REDSTONE ARSENAL AL 35898-5000
1	JOHNS HOPKINS APPL PHYSICS LAB W D'AMICO 11100 JOHNS HOPKINS RD LAUREL MD 20723-6099
3	US ARMY AMRDEC AMSAM SS AT L AUMAN R W KRETZSHMAR E VAUGHN REDSTONE ARSENAL AL 35898-5000
1	COMMANDER US ARMY ARDEC AMSRD AAR AEM A G MALEJKO BLDG 95 PICATINNY ARSENAL NJ 07806-5000
1	COMMANDER US ARMY ARDEC AMSRD AAR AEP E D CARLUCCI BLDG 94 PICATINNY ARSENAL NJ 07806-5000
1	COMMANDER US ARMY ARDEC ATTN WEI-JEN SU AEROBALLISTICS DIV PICATINNY ARSENAL NJ 07806-5000
1	BAE SYSTEMS R BURETTA CODE 170 4800 EAST RIVER RD MINNEAPOLIS MN 55421

NO. OF
COPIES ORGANIZATION

ABERDEEN PROVING GROUND

1 COMMANDER
US ARMY ARDEC
FIRING TABLES & BALLISTICS DIV
AMSRD AAR AEF T
F MIRABELLE
2201 ABERDEEN BLVD
APG MD 21005-5001

27 DIR USARL
AMSRD ARL WM B
M ZOLTOSKI
J NEWILL
AMSRD ARL WM BA
D LYON
AMSRD ARL WM BC
P PLOSTINS
J SAHU
M BUNDY
I CELMINS
M CHEN
G COOPER
J DESPIRITO
F FRESCONI
J GARNER
B GUIDOS
K HEAVEY
B HOWELL
X HUANG
S SILTON
P WEINACHT (3 CPS)
AMSRD ARL WM BD
B FORCH
M NUSCA
P CONROY
AMSRD ARL WM BF
W OBERLE
AMSRD ARL WM MB
T BOGETTI
W DRYSDALE
M MINNICINO